Atmospheric Environment 252 (2021) 118338

Contents lists available at ScienceDirect

Atmospheric Environment

journal homepage: http://www.elsevier.com/locate/atmosenv

Sources and characteristics of light-absorbing fine particulates over Delhi through the synergy of real-time optical and chemical measurements

Atinderpal Singh [a,1], Neeraj Rastogi [a,*], Varun Kumar [b], Jay G. Slowik [b], R. Satish [a], Vipul Lalchandani [c], Navaneeth M. Thamban [c], Pragati Rai [b], Deepika Bhattu [b], Pawan Vats [d], Dilip Ganguly [d], S.N. Tripathi [c], André S.H. Prévôt [b]

[a] Geosciences Division, Physical Research Laboratory, Ahmedabad, 380009, India
[b] Laboratory of Atmospheric Chemistry, Paul Scherrer Institute, 5232, Villigen PSI, Switzerland
[c] Department of Civil Engineering, Indian Institute of Technology, Kanpur, Uttar Pradesh, 208016, India
[d] Centre for Atmospheric Sciences, Indian Institute of Technology, New Delhi, 110016, India

HIGHLIGHTS

- Absorption characteristics and sources of brown carbon (BrC) are investigated.
- BrC contributed considerably to total absorption (23%) at 370 nm.
- The biomass burning OA exhibited the highest mass absorption efficiency.
- The low volatile oxygenated OA has virtually no contribution to BrC absorption.
- Around ~48% of BrC absorption is caused by biomass burning aerosol.

ARTICLE INFO

Keywords:
Carbonaceous aerosol
Brown carbon
Black carbon
Absorption
PMF
Megacity
India

ABSTRACT

This study examines the light absorption characteristics of fine atmospheric particulates using the co-located real-time measurements of chemical and optical aerosol characteristics at a site located in Delhi during winter. The contribution of absorption by black carbon and brown carbon (BC and BrC) to the total absorption (b_{abs}) is computed using the absorption Ångström exponent (AAE) method. The period average contribution of BrC absorption (b_{abs_BrC}) to b_{abs} is found to be highest at 370 nm (23%) that decreased exponentially with increasing wavelengths, i.e.,18, 12, 10, and 4% at 470, 520, 590, and 660 nm, respectively. The absorption spectrum of BrC is used to study the bulk composition of BrC, which indicates that primary BrC was dominant during morning and night time, whereas secondary BrC was significant during the rest of the time. Further, organic aerosols (OA) were divided into different factors using positive-matrix factorization (PMF) analysis, and the mass absorption efficiency (E_{abs}) of each factor was assessed through multivariate linear regression of b_{abs_BrC} with OA factors. The biomass burning OA (BBOA) exhibited the highest E_{abs} at 370 nm (0.86 $m^2\ g^{-1}$), followed by semi-volatile oxygenated OA (SVOOA; 0.67 $m^2\ g^{-1}$) and hydrocarbon-like OA (HOA; 0.42 $m^2\ g^{-1}$). Further, although the composition of OA was dominated by LVOOA (32%) and BBOA (32%), followed by SVOOA (22%), and HOA (14%), their contribution to b_{BrC} followed different order due to differences in their mass absorption efficiencies. The BBOA contributed almost half (48%) of b_{abs_BrC} followed by SVOOA (26%), and HOA (10%). This study provides quantitative information on the sources of BrC and their relative contribution to BrC absorption over a heavily polluted region, which is still lacking in the literature. These results have implications in understanding the source-specific BrC absorption.

* Corresponding author.
E-mail address: nrastogi@prl.res.in (N. Rastogi).
[1] Now at: Department of Environmental Studies, University of Delhi, Delhi 110007, India.

https://doi.org/10.1016/j.atmosenv.2021.118338
Received 15 October 2020; Received in revised form 23 February 2021; Accepted 6 March 2021
Available online 13 March 2021

1. Introduction

Carbonaceous aerosols are mainly comprised of black carbon (BC) and organic carbon (OC) that contribute considerably to the global climate. Until recently, it was believed that BC was the only light-absorbing aerosol component that leads to positive radiative forcing, and OC was considered to be a scattering-type aerosol (Andreae and Gelencsér, 2006). However, recent studies reported that some fraction of organics also shows light absorption characteristics from the near UV to the visible region, labeled as brown carbon (BrC) (Kirchstetter et al., 2004). Both the BC and BrC come from numerous sources including biomass burning (BB) emissions and fossil fuel combustion. The emissions from BB are the dominant source of BC on a global scale (Andreae, 2019), and the dominant source of BrC on a regional as well as global scale (Laskin et al., 2015 and references therein). BC is released directly into the atmosphere (Singh et al., 2016), while BrC can either be released directly into the atmosphere or formed through secondary processes (Cheng et al., 2011; Laskin et al., 2015). In comparison to BC, the properties of BrC are least understood as they may consist of thousands of organic compounds with complicated molecular compositions. BrC is identified as one of the significant contributors to climate forcing over the regions affected by BB emissions (Feng et al., 2013). The recent estimations displayed that the BrC contribution to the light absorption is around 27–70% of that from BC over different geographical regions worldwide (Lin et al., 2014; Wang et al., 2014). Furthermore, it is found that the direct radiative forcing at the top of the atmosphere due to organic aerosol can change from cooling (-0.08 Wm^{-2}) to warming ($+0.025$ Wm^{-2}) when strong BrC absorption is incorporate in global climate models (Feng et al., 2013). However, uncertainties involved in assessing the characteristics of BrC hinder more precise approximations of aerosol radiative forcing. In recent years, the studies on BrC aerosols increased substantially and most of them utilized real-time aerosol absorption properties to assess BrC characteristics (Qin et al., 2018; Zhang et al., 2020). Further, Zhang et al. (2020) documented the contribution of BrC to total absorption over the nine sites of France during the winter season using Aethalometer data. They reported that the contribution of BrC to total absorption varied from 18 to 42%, and stated that the majority of BrC come from wood-burning emissions. Shamjad et al. (2016) used the online measurements of aerosol absorption coefficients along with modeled data to assess the BrC properties over a polluted city Kanpur (India), and reported that BrC contributes ~30% to total absorption.

Rapid urbanization and industrialization in and around Delhi, a megacity and the capital of India led to severe air quality problems in this region, especially during winter (Rai et al., 2020). During winter, the long-range transport of biomass burning aerosols from the upwind locations, i.e., Punjab and Haryana, also contribute significantly to aerosol loading over Delhi (Bikkina et al., 2019). Furthermore, meteorological conditions play a vital role in the winter haze over Delhi, in addition to emissions from numerous sources (Sembhi et al., 2020). High loadings of carbonaceous aerosols are often recorded over Delhi during winter with a high fraction of organics (Tiwari et al., 2013; Gani et al., 2019; Puthussery et al., 2020). The higher concentrations of organics over Delhi indicate that the absorption due to BrC cannot be ignored. Recently, Dasari et al. (2019) studied the effect of photochemical aging on the absorption of BrC in south Asian outflow by considering Delhi as one of the sampling sites. They reported the mass absorption efficiency of 2.5 m^2g^{-1} for water-soluble BrC at Delhi. In another report from Delhi, the mass absorption efficiency of 1.6 m^2g^{-1} for water-soluble BrC is reported (Kirillova et al., 2014). However, the quantitative information on the sources and chemical composition of BrC over Delhi still lacks in the literature.

In this work, the measurements of the seven-wavelength Aethalometer have been utilized to quantify the contribution of BC and BrC to the total aerosol light absorption in the megacity of Delhi, which is among the highest polluted cities of the world. In addition to Aethalometer, the concurrent measurements have also been made with a high-resolution time-of-flight aerosol mass spectrometer (HR-ToF-AMS). Sources of organic aerosol (OA) were identified by performing the positive matrix factorization (PMF) analysis on highly time-resolved OA data measured using HR-ToF-AMS and correlated with the absorption coefficient of BrC to investigate the major contributors to BrC absorption. Further, the mass absorption efficiency of each OA factor is estimated.

2. Materials and methods

2.1. Site description

This study was carried out by deploying real-time aerosol measurement instruments on the fourth floor of the building (at the height of ~15 m above ground level) inside the campus of the Indian Institute of Technology Delhi (28.54°N, 77.19°E; Fig. S1) in South Delhi during winter (January 01 to February 10, 2019). Delhi, the capital of India, experiences substantial emissions from various sources, resulting in high aerosol loading (Gani et al., 2019; Dumka et al., 2019; Rai et al., 2020; Wang et al., 2020). This is one of the megacities of South Asia with a population of ~17 million and average population density of ~11,320 people km^{-2} in 2011 (Rai et al., 2020 and references therein). The air quality of Delhi is affected by emissions from numerous anthropogenic sources, including power plants (2 coal-based and 4 natural gas-based), vehicles, industrial (~29 medium and small-scale industries and 5 factory complexes), and brick kilns in the surrounding regions (Guttikunda and Calori, 2013). In addition to these sources, the long-range transport of aerosols from several hundreds of kilometers of upwind regions also contributes to the air pollution of Delhi. A recent study reported that ~42% of BC during winter over Delhi comes from the regional transport of biomass/wood burning emissions from the upwind rural regions of Haryana and Punjab (Bikkina et al., 2019). The meteorological data were obtained from the automatic weather station installed at the same site and atmospheric boundary layer height data was acquired through the NOAA-HYSPLIT model. The detailed site description was reported elsewhere (Puthussery et al., 2020; Rai et al., 2020; Wang et al., 2020).

2.2. Aethalometer measurements

The aerosol light absorption and corresponding equivalent BC was monitored online at seven wavelengths i.e., 370, 470, 520, 590, 660, 880, and 950 nm at the interval of one minute using a dual-spot Aethalometer (AE33, Magee Scientific; Hansen et al., 1984; Drinovec et al., 2015). Aethalometer measured aerosol light absorption coefficient (b_{abs}) at seven wavelengths and converts it into the BC concentration in real-time using the constant mass absorption cross-section (MAC) of 18.47, 14.54, 13.14, 11.58, 10.35, 7.7 and 7.19 m^2 g^{-1} for these seven wavelengths. These measurements are corrected for filter loading artifacts and tape advancement error (Drinovec et al., 2015). The absorption coefficient at 880 nm is used for the BC estimation as it is the major absorber at 880 nm (Yang et al., 2009). Here, it is supposed that the absorption is primarily due to carbonaceous aerosol, and the contribution of dust is negligible because this BC was measured in the particulate matter having an aerodynamic diameter less than or equal to 1 μm (PM_1; PM_1 cyclone was installed at the inlet of sampling line). This study period was also not subjected to any dust event which was evident from the absence of any major enhancement in dust aerosols over Delhi during the same study period (Rai et al., 2020).

The relative contribution of absorption due to BrC (b_{abs_BrC}) and BC (b_{abs_BC}) to the total aerosol absorption (b_{abs}) is estimated using a method suggested by Lack and Langridge (2013). The absorption due to BrC at short wavelength ($b_{abs\_BrC,\ \lambda1}$) is estimated by subtracting the absorption of BC ($b_{abs\_BC,\ \lambda1}$) from the total absorption as follows:

$$b_{abs\_BrC,\lambda1} = b_{\lambda1} - b_{abs\_BC,\lambda1} \quad (1)$$

where absorption $b_{\lambda 1}$ is the total absorption at wavelength λ1 and absorption due to BC at λ1 is estimated using the AAE value of BC (AAE_{BC})

$$b_{abs\_BC,\lambda 1} = b_{\lambda 2} \times \left(\frac{\lambda_2}{\lambda_1}\right)^{AAE_{BC}} \quad (2)$$

where $b_{\lambda 2}$ is the absorption at a higher wavelength (880 nm). Here, it is assumed that there is no contribution to light absorption by BrC and dust at 880 nm (Zhu et al., 2017). The choice of AAE_{BC} (= 1) while estimating the b_{BC} is one of the primary sources of uncertainty, as AAE_{BC} usually varies between 0.9 and 1.1 (Lu et al., 2015). A sensitivity test was performed using the AAE_{BC} values of 0.9, 1.0, and 1.1, respectively to assess the impact of different AAE_{BC} values on the quantification of BrC (Fig. S2). The result of the sensitivity test indicates that the percentage change in b_{abs_BrC} (at 370 nm) is about ±25% if the different values of AAE_{BC} are used.

2.3. HR-ToF-AMS measurements and source apportionment method

In parallel, the HR-ToF-AMS (Aerodyne Inc, USA) was also operated that measured non-refractory PM_1 (NR-PM_1), composed of OA, SO_4^{2-}, NO_3^-, NH_4^+ and Cl^-, in real-time at the interval of two minutes. It was operated in the highly sensitive V mode, and all the required calibrations such as particle velocity, ionization efficiency (IE), and inlet flow performed using well-known standard protocols (Canagaratna et al., 2007). The mass-based IE calibration was done using 300 nm ammonium nitrate particles, and the default RIEs mentioned by Canagaratna et al. (2007) were utilized in this analysis. The ammonium nitrate particles of different diameters are used to derive the empirical parameters of the velocity equation. The standard toolkits named SQUIRREL (SeQUential Igor data RetRiEvaL) and PIKA (Peak Integration by Key Analysis) written in IGOR (Wavemetrics, Inc., Lake Oswego) were used to analyze the HR-ToF-AMS data (Canagaratna et al., 2007). The raw data is processed with the standard fragment table (Allan et al., 2004). However, to eliminate the contributions of gas-phase CO_2 from the measured CO_2^+ (m/z = 44) signal, a small adjustment was made (Singh et al., 2019). The elemental ratios of OA (O/C, H/C) and organic matter to organic carbon (OM/OC) ratio were derived with an improved-ambient method (Canagaratna et al., 2015). More details about the calibrations procedure and data processing are provided in our earlier publication (Rastogi et al., 2019; Singh et al., 2019).

Source apportionment of OA mass spectra was performed using the positive matrix factorization (PMF) model (Paatero and Tapper, 1994). The Multilinear Engine-2 (ME-2) algorithm (Paatero, 1999) was used to solve the PMF model and was implemented using the Source Finder (SoFi, Datalystica Ltd., Villigen, Switzerland) interface version 6.6 (Canonaco et al., 2013). To explore the rotational ambiguity, The SoFi/ME-2 package allows the use of a priori information in the PMF analysis, so that elements of either the G and/or F matrix can be constrained from known factor profiles and/or factor time series. This is known as a-value approach. A total of five OA factors were identified in the PMF analysis, which were hydrocarbon like OA (HOA), biomass burning OA (BBOA1 and BBOA2), semi-volatile oxygenated OA (SVOOA), and low-volatile oxygenated OA (LVOOA). More information on the PMF analysis is provided in the supplement document (Fig. S3).

3. Results and discussion

3.1. Characteristics of light-absorbing species (BC and BrC)

Fig. 1 displays the temporal variation in mass concentrations of BC at 370 nm (BC_{370} also known as UVPM) and 880 nm (BC_{880}) during the whole campaign. Large variability was recorded in the mass concentration of BC_{370} (1.3–113 μg m^{-3}) and BC_{880} (1.0–90 μg m^{-3}) with a period average of 21 ± 17 μg m^{-3} (avg ± 1σ) and 16 ± 13 μg m^{-3}, respectively, over Delhi. These variations can be attributed to many

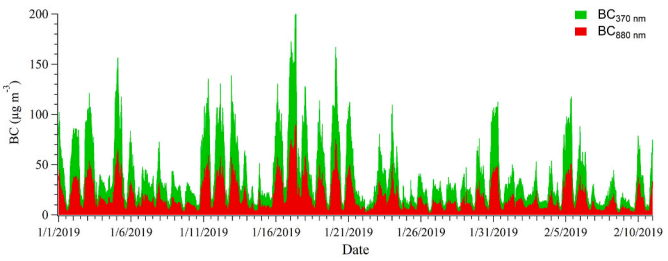

Fig. 1. Temporal variation in concentrations of BC_{370} and BC_{880} aerosols (concentrations are stacked).

parameters, such as temporally varying sources, regional transport patterns, atmospheric processing, and meteorological conditions. This study was conducted during winter so the shallower atmospheric boundary layer (<200 m except for noon hours, Fig. S4) also favors the accretion of the particles near the surface. Earlier studies from the same region also reported the high aerosol loading events during winter due to heavy local pollution, regional transport, and stagnant atmospheric conditions (Bikkina et al., 2019; Gani et al., 2019; Rai et al., 2020). During winter, the regional transport from upwind locations also contributes significantly (around 42%) to the ambient BC concentrations along with local sources over Delhi (Bikkina et al., 2019).

Fig. 2 depicts the diurnal variation in the BC_{370} and BC_{880} that provides deeper understandings of the effect of sources and atmospheric processes on BC_{370} and BC_{880} abundances. The BC at 370 and 880 nm displayed a significant diurnal cycle with higher concentrations during the morning and evening hours, which overlap with traffic rush hours. The BC at both the wavelengths showed a similar diurnal variation except during the evening hours, where a relatively higher rate of change was observed in BC_{370}, which is also reflected in the $BC_{370/880}$ mass ratio. A relatively high $BC_{370/880}$ mass ratio during evening time suggested that the biomass burning emissions/residential wood-burning can significantly contribute to the evening peak of BC (Herich et al., 2011; Rastogi et al., 2020), in addition to vehicular emissions (Fig. 2). The boundary layer dynamics also favor the accretion of the particles close to the Earth's surface during the morning and evening hours (Fig. S4). BC exhibited lower concentrations during the middle of the day probably because of the collective effects of reduced vehicular emissions and extended atmospheric boundary layer (Fig. 2 and S4). It is interesting to note that the concentrations of BC remained on the higher side during the mid-night hours. The higher concentrations of BC during the night time could be due to the fresh local emissions from diesel trucks as their entry to Delhi is banned from 07:00–21:00 LT (Wang et al., 2020). This inference is supported by the observed decrease in $BC_{370/880}$ mass ratio from mid-night till morning (Fig. 2). Furthermore, the contribution of traffic and biomass burning emissions to ambient BC

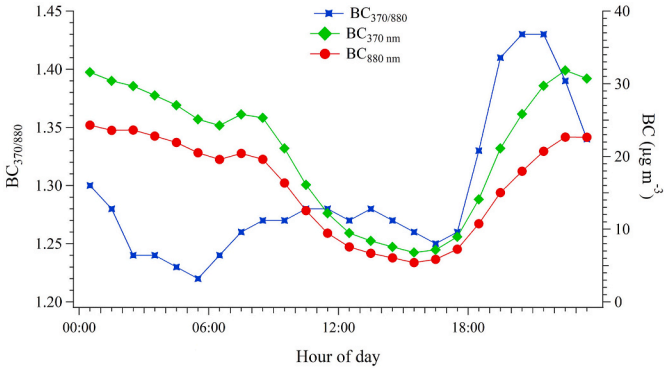

Fig. 2. Diurnal variation in BC_{370} and BC_{880} concentrations, and $BC_{(370/880)}$ mass ratio.

is estimated using the spectral dependence of light absorption by the BC coming from the different sources (Sandradewi et al., 2008; Pani et al., 2020). The diurnal variations in the biomass burning derived BC (BC_{BB}), BC coming from traffic ($BC_{Traffic}$), and the relative contribution of $BC_{Traffic}$ to BC_{BB} are shown in Fig. S5. The relative contribution of $BC_{Traffic}$ in comparison to BC_{BB} exhibited an increasing trend during mid-night hours and the mass concentration of $BC_{Traffic}$ also remained high during these hours, which supports our earlier argument related to the nocturnal impact of diesel tracks on the ambient BC. The morning traffic peak and the impact of BB emissions on the concentration of ambient BC during late evening hours are reflected in the diurnal variation of $BC_{Traffic}/BC_{BB}$ mass ratio (Fig. S5).

Furthermore, the Aethalometer measurements at seven wavelengths were used to estimate the spectral absorption coefficient (b_{abs}) during the study period, as shown in Fig. 3. In this study, the mean value of b_{abs} is found to be 181, 135, 113, 96, 81, 58 and 54 Mm^{-1} ($1M = 10^{-6}$) at 370, 470, 520, 590, 660, 880 and 950 nm, respectively over the study site. The values of b_{abs} decreased exponentially with an increasing wavelength (from 370 to 950 nm) as evident from Fig. 3. A similar variation in spectral b_{abs} is reported by several researchers across the globe for ambient measurements (Singh et al., 2014; Massabò et al., 2015; Ran et al., 2016). The value of b_{abs} (58 Mm^{-1} at 880 nm) over Delhi is significantly higher than that observed over Patiala (27 Mm^{-1} at 880 nm) during winter, a site located in the upwind direction of Delhi (Singh et al., 2014). It highlights the severity of pollution levels over Delhi. The wavelength dependence of b_{abs} is usually given by a power law and the exponent of the power-law fitting is termed as AAE (Ramana et al., 2010; Singh et al., 2014). In this study, the values of b_{abs} over seven wavelengths (370–950 nm) are fitted using power law, and the corresponding values of AAE varied from 0.96 to 1.66 (1.27 ± 0.10; average ± 1σ). The wavelength dependence of b_{abs} gives an idea about the sources, as the magnitude of AAE varies for different sources. The AAE value of unity is often used for pure black carbon, around 2 for the aerosol from savanna biomass burning (Kirchstetter et al., 2004), and greater than 2 for mineral dust (Russell et al., 2010). Singh et al. (2014) reported an AAE of 1.5 for paddy residue burning in Punjab state which is located in the upwind of the present study region. The values of AAE higher than unity also represent the presence of brown carbon (BrC) because BrC exhibit considerable absorption in UV and near short visible wavelengths than that at longer wavelengths (Andreae and Gelencsér, 2006; Bergstrom et al., 2007). The frequency distribution of AAE obtained in this study is skewed towards the higher values (>1) with a mean value of 1.27, which indicates a significant presence of BrC over the study region (Fig. S6), which is also discussed in the literature (Andreae and Gelencsér, 2006; Bergstrom et al., 2007; Bikkina et al., 2016; Choudhary et al., 2018). Moreover, AAE displayed a noticeable diurnal variation, which reflects the variability in the sources of absorbing carbonaceous species throughout the day (Fig. S7). The AAE during the day time {07:00 to 18:00 local time (LT)} was ~1.27, which was close to the mean value of AAE during the sampling period. However, AAE values were minimum at 05:00 and 17:00 LT and peaked between 19:00–21:00 LT (AAE ~1.4). The significant higher value of AAE from 19:00 to 21:00 LT and marginal increase in AAE values during the 06:00 to 16:00 LT could be due to the increase in the relative contribution of biomass burning emissions/residential wood-burning which is supported by a higher $BC_{370/880}$ mass ratio at the same time (Fig. 2). The lowest AAE values during the morning and evening hours (around 05:00 LT and 17:00 LT) were attributable to a decrease in UVPM (BC_{370}; related with biomass burning emissions/residential wood-burning) relative to BC_{880} at the same time (Fig. 2). The emissions from diesel trucks could be a possible reason for the decline in the magnitudes of AAE after mid-night hours. The AAE exhibited a decreasing trend under the influence of traffic emissions and showed the enhancement under the impact of biomass burning emissions/residential wood-burning. It is also supported by the variation of $BC_{Traffic}/BC_{BB}$ ratio (Fig. S5).

The spectral absorption pattern of b_{abs_BrC} and b_{abs_BC} suggests that BC is the dominant light absorber at all wavelengths whereas BrC contributed considerably to total absorption at shorter wavelengths (Fig. 4). The mean fraction of b_{abs_BrC} to total absorption (b_{abs}) during the sampling period is found to be 23, 18, 12, 10, and 4% at 370, 470, 520, 590, and 660 nm, respectively, during the present study. The contribution of b_{abs_BrC} to total absorption (b_{abs}) during this study is similar to a report from a suburban site downwind of Guangzhou, China (Qin et al., 2018). For further investigation, the absorption at 370 nm is considered as the BrC absorption, which is more prominent at 370 nm as compared to other wavelengths (Laskin et al., 2015 and references therein). Diurnal variation of b_{abs_BrC} and b_{abs_BC} at 370 nm displayed a similar trend from 07:00 to 18:00 LT (Fig. 5). In contrast to the diurnal cycle of b_{abs_BrC} and b_{abs_BC} at 370 nm, the relative contribution of b_{abs_BrC} and b_{abs_BC} to total b_{abs} at 370 nm exhibited the opposite trend

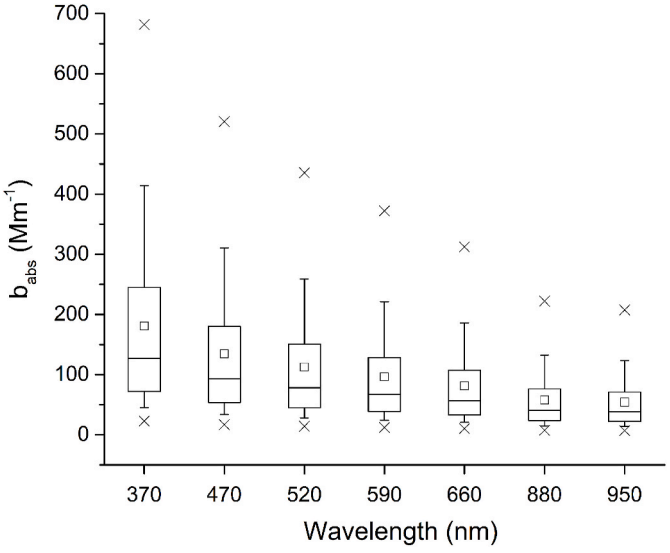

Fig. 3. Spectral variation of absorption coefficient (b_{abs}) during the study period. The boundary of the box closest to zero indicates the 25th percentile, a line within the box represents the median, and the boundary of the box farthest from zero indicates the 75th percentile. Error bars above and below the box indicate the 90th and 10th percentiles. Cross marks closest to zero and farthest from zero are indicative of the 1st and 99th percentile, respectively.

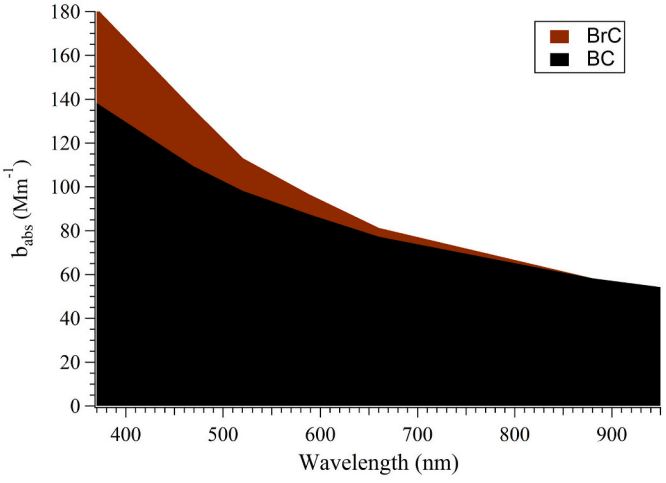

Fig. 4. Average absorption coefficient (b_{abs}) of black carbon (BC) and brown carbon (BrC) during the observation period. (For interpretation of the references to colour in this figure legend, the reader is referred to the Web version of this article.)

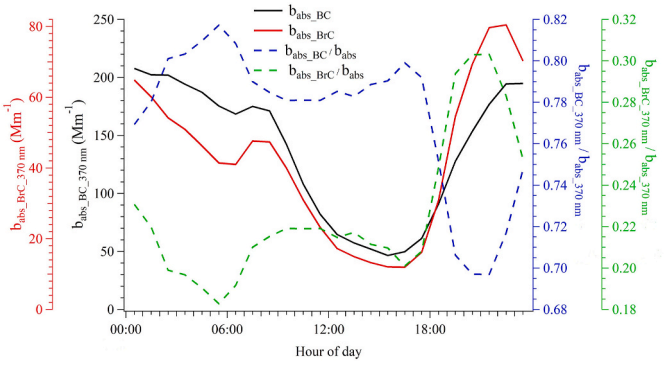

Fig. 5. Diurnal variations in absorption coefficient (b_{abs}) of black carbon (BC) and brown carbon (BrC), and their relative contributions to the total absorption coefficient (b_{abs}) at 370 nm. (For interpretation of the references to colour in this figure legend, the reader is referred to the Web version of this article.)

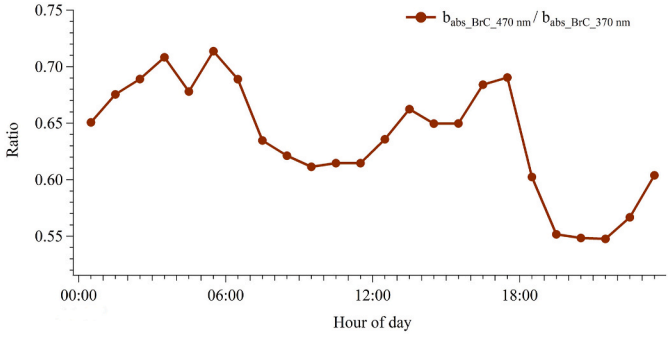

Fig. 6. Diurnal variation in the ratio of absorption coefficient (b_{abs}) of brown carbon (BrC) at 470 to 370 nm. (For interpretation of the references to colour in this figure legend, the reader is referred to the Web version of this article.)

(Fig. 5). Fig. 5 depicts the contribution of b_{abs_BC} to total b_{abs} at 370 nm which start increasing after mid-night and attained the highest fraction (around ~82%) in the morning at 06:00 LT and again start decreasing in the afternoon hours with a small increase from 15:00 to 17:00 LT. There was a steep decrease in b_{abs_BC}/b_{abs} during the evening to night time (18:00 to 21:00 LT), and it attained the lowest fraction of ~69%, and after that, it increases till 06:00 LT. In both cases, drastic changes in the fraction to total absorption has occurred during late evening hours (Fig. 5). This enhancement in b_{abs_BrC}/b_{abs} is likely due to an increase in the relatively higher contribution of BB-derived aerosols during late evening hours which is also indicated by the enhancement in $BC_{370/880}$ and $BC_{Traffic}/BC_{BB}$ mass ratio during that time (Fig. 2 and S5). Despite an increase in b_{abs_BrC}/b_{abs} ratio at 370 nm during late evening hours, BC has still higher absorption than the BrC at 370 nm and also at other wavelengths, suggesting that BC is the dominant absorbing component of absorbing carbonaceous aerosols.

3.2. Primary versus secondary BrC

The BrC may consist of thousands of organic compounds and every compound may have diverse absorbing characteristics. Analytically, it is extremely difficult to assess all the distinct BrC species and their optical characteristics. Therefore, researchers often study the absorption coefficient at a certain wavelength as a measure of BrC. Recently, Satish and Rastogi (2019) used the absorption spectrum of BrC to assess their broader composition over a semi-urban city of India. Although this method is not the replacement of performing molecular speciation of BrC, it is useful in identifying the bulk composition. This method is based on the idea that BrC chromophores absorption is wavelength-specific (Kirchstetter et al., 2004; Lukács et al., 2007; Lin et al., 2015). Thus, the ratio of b_{abs_BrC} of a sample normalized to reference (or other) sample at different wavelengths gives an idea about the BrC bulk composition. Earlier studies reported that b_{abs_BrC} at 365 nm is mainly due to HULIS type BrC (generally primary origin) and absorption at >400 nm is likely due to nitroaromatic-type BrC (mostly secondary origin) (Lukács et al., 2007; Lin et al., 2015; Xie et al., 2017). Earlier studies suggested that most of the water-soluble HULIS type compounds are bounded with the submicron particulates (Lin et al., 2010), so HULIS type BrC was also expected in a considerable amount during present study.

The diurnal variability in the ratio of b_{abs_BrC} at 470 nm to the 370 nm (b_{abs_BrC} (470/370)) is shown in Fig. 6. In this study, we assumed that the observations of b_{abs_BrC} at 370 nm represent the absorption due to HULIS like compounds, and at 470 nm is caused by nitro-aromatic-type BrC, similar to the method proposed by Satish et al. (2017). Thus, the present discussion mainly focuses on the variability in HULIS-type BrC versus nitro polycyclic aromatic hydrocarbons (PAHs) BrC. If BrC was from one source only, then it is anticipated that the ratio of spectral absorbance (370/470) would be the same at different times of the day. Fig. 6 depicted that there was substantial diurnal variability in b_{abs_BrC} (470/370) ratio which indicates that the BrC sources were not uniform throughout a day over the study region. The b_{abs_BrC} (470/370) ratio decreased during the morning (~07:00–12:00 LT) and evening hours (~19:00–22:00 LT). A decline in the ratio during morning hours matched well with rush hours when the primary emissions from vehicles are expected. However, such a trend was not observed during the evening rush hours (17:00–18:00 LT). It could be due to the abundance of nitro-PAHs during that time which absorbs visible light efficiently (Yu, 2002), or these BrC species may be photosensitive. The b_{abs_BrC} (470/370) ratio also displayed enhancement during early morning hours (~02:00–06:00 LT) and afternoon to evening hours (~14:00–18:00 LT). The increase in b_{abs_BrC} (470/370) ratio during ~14:00–18:00 LT suggests the photochemical formation of secondary BrC whereas nocturnal oxidants may be accountable for the early morning peak. This study was carried out during the winter when the people of this region often using the bonfire (usually burn biofuel, wood, coal, etc.) to keep themselves warm during the cold morning and evening hours. The b_{abs_BrC} (470/370) ratio displayed an interesting diurnal cycle which warrants further investigation. Overall, it indicates that primary BrC (mainly HULIS like compound) was dominant during morning and night time whereas secondary BrC was significant during the rest of the time.

3.3. The contribution of different sources to BrC absorption

During this study, the HR-ToF-AMS was also run simultaneously along with the Aethalometer. Similar to the BC, the AMS measurements ($NR\text{-}PM_1$) also recorded a strong variability in the mass concentration of OA (7.2–468 μg m^{-3}), SO_4^{2-} (3.7–114 μg m^{-3}), NO_3^- (2.0–64 μg m^{-3}), NH_4^+ (3.7–102 μg m^{-3}) and Cl^- (0.2–186 μg m^{-3}) during the study period. The composition of $NR\text{-}PM_1$ is dominated by OA, contributing on average ~47% to the total $NR\text{-}PM_1$ mass, followed by NH_4^+ (16%), NO_3^- (14%), SO_4^{2-} (13%), and Cl^- (10%). The dominance of OA in $NR\text{-}PM_1$ composition observed in this study is consistent with the earlier reported studies, showing ubiquitous dominance of organics in fine particles (Hallquist et al., 2009; Zhang et al., 2011; Hu et al., 2016; Singh et al., 2019; Thamban et al., 2019). After OA, the composition of $NR\text{-}PM_1$ is dominated by NH_4^+ which was sufficient to neutralize all the acidic ions (SO_4^{2-}, NO_3^-, and Cl^-) (Fig. S8). It is important to mention here that the aerosol neutralization ratio is estimated by presuming NH_4^+ is the only predominant cation in submicron size. It further indicates that NH_4^+ was the major cation forming secondary inorganic salts such as NH_4NO_3, $(NH_4)_2SO_4$, and NH_4Cl (Zhang et al., 2007). Exceptionally high mass fraction and concentrations of Cl^- were also recorded (0.2–186 μg m^{-3}) during this study, consistent with the earlier study from Delhi (Gani et al., 2019; Tobler et al., 2020). Ambient Cl^- concentrations observed

over the study region is one of the highest recorded concentrations of Cl^- worldwide. The emissions from 2 coal-based power plants and waste combustion yards along with regional transport of biomass burning smoke could be the source of HCl over Delhi (Crisp et al., 2014). Co-variability of NH_4^+ and Cl^- suggests that the Cl^- was likely neutralized by the NH_3 alone to form the NH_4Cl under the favorable meteorological condition (high RH and low temperature), which is corroborated by the decreasing concentration of Cl^- with increasing temperature, as NH_4Cl is a volatile compound (Ianniello et al., 2011).

To assess the relation between OA factors and b_{abs_BrC} at 370 nm, the correlation between these factors and b_{abs_BrC} at 370 nm is investigated. The b_{abs_BrC} displayed a strong correlation with most of the PMF factors such as HOA ($r^2 = 0.70$), BBOA1 ($r^2 = 0.64$) and BBOA2 ($r^2 = 0.78$), and moderate correlation with SVOOA ($r^2 = 0.48$) (Fig. S9). However, the LVOOA exhibited a very poor correlation with b_{abs_BrC} ($r^2 = 0.01$). It suggests that oxidized or aged OA does not contribute to BrC absorption significantly. This type of poor relationship between LVOOA and b_{abs_BrC} was also reported earlier over the Indian city Kanpur (Satish et al., 2017). Further, the relationship between components of OA provided by PMF and the b_{abs_BrC} was utilized to assess the role of each factor in the BrC absorption (mass absorption efficiency of each factor). In this analysis, the BBOA factor represents the combination of both BBOA1 and BBOA2. The LVOOA factor is excluded from the analysis due to its negligible contribution towards BrC absorption, as also evident from their poor correlation with b_{abs_BrC} (Fig. S9). The total absorption coefficient of OA (i.e. BrC) is the summation of the absorption coefficient of the n parts of the OA (de Sá et al., 2019):

$$b_{abs\_BrC} = b_{abs\_OA1} + b_{abs\_OA2} + b_{abs\_OA3} + \dots\dots\dots + b_{abs\_OAn} \quad (3)$$

Here, we assumed the nonappearance of cross-interactions between the parts and it holds for a single wavelength. The absorption coefficient $b_{abs,i}$ of part i as follows:

$$b_{abs,i} = E_{abs,i} * C_i \quad (4)$$

where $E_{abs,i}$ is the mass absorption efficiency and C_i is the mass concentration of part i (in μg m^{-3}). By combining the above two equations, the following equation was constructed

$$b_{abs\_BrC} = E_{abs,\ HOA}G_{HOA} + E_{abs,\ BBOA}G_{BBOA} + E_{abs,\ SVOOA}G_{SVOOA} + B \quad (5)$$

where G_i refers to the concentration of factor i (in μg m^{-3}), and the unknowns are the mass absorption efficiencies $E_{abs,i}$ (in m^2 g^{-1}) related with these PMF factors. An intercept B corresponds to the variability not described by the PMF factors. Other studies also used this type of multivariate linear regression to assess mass absorption efficiencies (Ealo et al., 2018). The highest value of E_{abs} at 370 nm, assessed through multivariate linear regression of b_{abs_BrC} on OA factors as per equation (5), is observed for BBOA (0.86 m^2 g^{-1}), followed by SVOOA (0.67 m^2 g^{-1}) and HOA (0.42 m^2 g^{-1}), reflecting the characteristics of BrC coming from these source factors. The intercept of the analysis is found to be 6.75 Mm^{-1}. This absorption of BrC is not explained by the OA components likely because the statistical model does not consider the physical process such as mixing state etc. The multi-collinearity between these PMF factors (excluding LVOOA) is also checked using the variance inflation factor (VIF) (Table S1). It is found that BBOA and HOA showed moderate correlation with other factors (VIF is in the order of 5). However, there is no problem of multi-collinearity in the case of SVOOA as VIF was close to unity. The existence of multi-collinearity in the case of BBOA and HOA could be due to their primary nature and it is one of the limitations of this regression model. The E_{abs} of 0.82 and 1.50 m^2 g^{-1} at 370 nm is reported for more oxidized BBOA and less oxidized BBOA, respectively, over central Amazonia (de Sá et al., 2019). The E_{abs} of BBOA (0.86 m^2 g^{-1}) in this study is very similar to that reported by de Sá et al. (2019) for more oxidized BBOA (0.86 m^2 g^{-1}). However, they observed significantly higher (2.04 m^2 g^{-1}) mass absorption efficiency in the case of HOA as compared to this study (0.42 m^2 g^{-1}), which could be due to differences in the HOA sources or meteorological factors. In another study by Xie et al. (2018), the E_{abs} of 0.62 m^2 g^{-1} at 365 nm is reported for gasoline vehicles. The highest mass absorption efficiency was observed for the biomass burning factor and lowest in the case of HOA in this study. The lower mass absorption efficiency of oxidized OA (SVOOA) is likely due to the photo-bleaching of the BrC compound (Bikkina et al., 2016; Satish et al., 2017).

Furthermore, the mass absorption efficiency of each factor is used to estimate the contribution of each factor in b_{abs_BrC} as per Equation (5). The composition of OA is dominated by LVOOA (32%) and BBOA (32%), followed by SVOOA (22%), and HOA (14%) (Fig. 7). However, their contribution to b_{abs_BrC} did not follow the same order due to differences in their mass absorption efficiencies as evident from Fig. 7. The LVOOA is the largest contributor to OA loading along with BBOA but it has virtually no contribution to BrC absorption. However, the high loading of LVOOA could be one of the major reasons behind the Delhi haze during winter due to their relatively more hygroscopic nature as compared to other OA components (Ng et al., 2011). On the other hand, biomass burning factors (sum of BBOA1 and BBOA2) shared the same fraction in OA mass (32%) as contributed by the LVOOA, but almost half of b_{abs_BrC} (48%) comes from biomass burning aerosol. The present study was conducted in the megacity where the number of vehicles is very high (~11 million in 2018; Rai et al., 2020). But their effect is not reflected in the contribution of HOA to b_{abs_BrC} (10%). It indicates that the primary OA coming from vehicular emissions has relatively less potential to absorb UV light compared to the biomass burning derived OA during winter. The SVOOA is the second largest contributor in OA loading and it has also displayed significant absorption (26%). The SVOOA also belongs to oxygenated aerosols similar to LVOOA but contained relatively less photochemical aged aerosol as compared to LVOOA which makes SVOOA more absorbing than that of LVOOA. All these factors accounted for 84% of b_{abs_BrC} and 16% comes from other factors that are not explained by PMF factors.

The understanding of light absorption due to OA is in the initial stage and most of the models considered OA as a purely scattering aerosol (Myhre et al., 2013). The results of this study state that the contribution of both urban and biomass burning emissions to OA absorption is significant. The recent estimations showed that the atmospheric radiative forcing due to water-soluble BrC is around 40% and methanol-soluble BrC is around 62% of that due to BC over a region dominated by

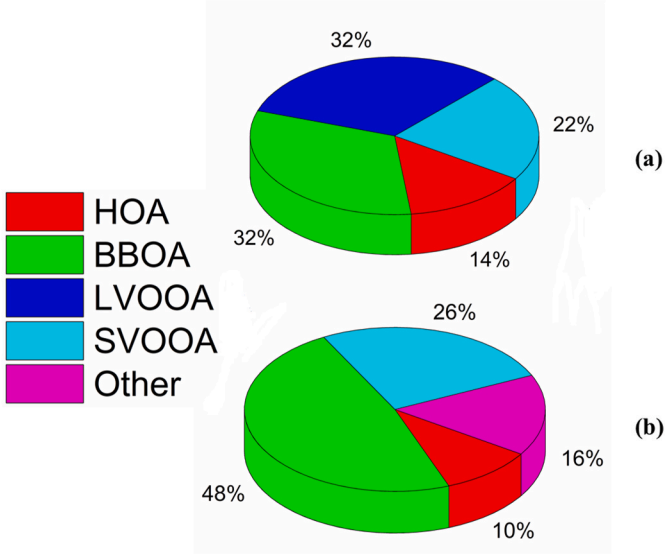

Fig. 7. The relative contribution of OA component loadings (a) to OA mass and (b) to brown carbon absorption at 370 nm (b_{abs_BrC}). (For interpretation of the references to colour in this figure legend, the reader is referred to the Web version of this article.)

biomass burning emissions (Bikkina et al., 2016; Satish et al., 2020). Thus, absorption due to OA should be included in the model to assess the actual impacts of aerosol on the climate.

4. Conclusions

The direct radiative forcing at the top of the atmosphere due to organic aerosol can change from cooling to warming when strong BrC absorption is incorporated in global climate models. However, to assess the precise impact of BrC on climate, a proper understanding of BrC absorption and its sources is very important. This study reports the absorption properties of fine particulates using the co-located measurements of Aethalometer and HR-ToF-AMS over Delhi during winter. Aethalometer measurements at seven wavelengths (370–950 nm) are used to estimate the spectral absorption coefficients (b_{abs}). Further, the b_{abs} is separated into absorption due to BrC (b_{abs_BrC}) and BC (b_{abs_BC}) using absorption Ångström exponent (AAE) method. On a diurnal scale, BrC exhibited higher absorption during late evening hours due to an increase in the contribution of BB derived aerosol at that time. However, BC showed overall higher absorption than BrC at all the wavelengths. Our results suggest that BrC composition is a mixture of at least HULIS and nitrogen-containing organic compounds over the study region. The OA, measured with HR-ToF-AMS, separated into their five components (BBOA1, BBOA2, HOA, SVOOA, and LVOOA) using PMF. The OA composition was dominated by LVOOA (32%) and BBOA (32%), followed by SVOOA (22%), and HOA (14%). BBOA is the major source of highly absorbing BrC and highly oxygenated OA (LVOOA) is relatively much less absorbing. Further, the mass absorption efficiency (E_{abs}) of each factor was assessed through multivariate linear regression of b_{abs_BrC} with OA factors. The biomass burning OA (BBOA1+BBOA2) exhibited the highest E_{abs} at 370 nm (0.86 $m^2\ g^{-1}$), followed by SVOOA (0.67 $m^2\ g^{-1}$) and hydrocarbon-like OA (HOA, 0.42 $m^2\ g^{-1}$). Further our results suggest that BBOA contributed almost half of b_{abs_BrC} (48%), followed by SVOOA (26%) and HOA (10%). Although the LVOOA was one of the dominant fractions of OA (32%), it has a negligible contribution to b_{abs_BrC}. These results have implications in understanding the source-specific BrC absorption which can further be used in adopting effective mitigation policies. These results also have implications in the regional climate models.

CRediT authorship contribution statement

Atinderpal Singh: Methodology, Software, Validation, Formal analysis, Investigation, Writing – original draft, Writing – review & editing. **Neeraj Rastogi:** Supervision, Resources, Writing – review & editing, Project administration. **Varun Kumar:** Methodology, Software, Validation, Formal analysis, Investigation, Writing – review & editing. **Jay G. Slowik:** Investigation, Writing – review & editing. **R. Satish:** Investigation, Writing – review & editing. **Vipul Lalchandani:** Methodology, Investigation, Software, Writing – review & editing. **Navaneeth M. Thamban:** Investigation, Writing – review & editing. **Pragati Rai:** Investigation, Writing – review & editing. **Deepika Bhattu:** Investigation, Writing – review & editing. **Pawan Vats:** Writing – review & editing. **Dilip Ganguly:** Resources, Writing – review & editing. **S.N. Tripathi:** Writing – review & editing, Project administration, Funding acquisition. **André S.H. Prévôt:** Investigation, Writing – review & editing, Project administration, Funding acquisition.

Declaration of competing interest

The authors declare that they have no known competing financial interests or personal relationships that could have appeared to influence the work reported in this paper.

Acknowledgments

We thank the Department of Biotechnology (DBT), Government of India, to conduct this research under grant no. BT/IN/UK/APHH/41/KB/2016-17 dated 19th July 2017 and financial support provided by Central Pollution control board (CPCB), Government of India, to conduct this research under grant number AQM/Source apportionment_EPC Project/2017). We thank the reviewers for their comments and suggestions in improving the quality of our manuscript.

Appendix A. Supplementary data

Fig. S1 to S9, Table S1, and discussion on VIF method and PMF SoFi factors are provided in the supplementary information.

Supplementary data to this article can be found online at https://doi.org/10.1016/j.atmosenv.2021.118338.

References

Allan, J.D., Delia, A.E., Coe, H., Bower, K.N., Alfarra, M.R., Jimenez, J.L., Middlebrook, A.M., Drewnick, F., Onasch, T.B., Canagaratna, M.R., Jayne, J.T., Worsnop, D.R., 2004. A generalised method for the extraction of chemically resolved mass spectra from aerodyne aerosol mass spectrometer data. J. Aerosol Sci. 35, 909–922.

Andreae, M.O., Gelencsér, A., 2006. Black carbon or brown carbon? The nature of light-absorbing carbonaceous aerosols. Atmos. Chem. Phys. 6, 3131–3148. https://doi.org/10.5194/acp-6-3131-2006.

Andreae, M.O., 2019. Emission of trace gases and aerosols from biomass burning – an updated assessment. Atmos. Chem. Phys. 19, 8523–8546. https://doi.org/10.5194/acp-19-8523-2019.

Bergstrom, R.W., Pilewskie, P., Russell, P.B., Redemann, J., Bond, T.C., Quinn, P.K., Sierau, B., 2007. Spectral absorption properties of atmospheric aerosols. Atmos. Chem. Phys. 7, 5937–5943. https://doi.org/10.5194/acp-7-5937-2007.

Bikkina, S., Rastogi, N., Sarin, M.M., Singh, A., Singh, D., 2016. Mass absorption efficiency of light absorbing organic aerosols from source region of paddy-residue burning emissions in the Indo-Gangetic Plain. Atmos. Environ 125, 360–370. https://doi.org/10.1016/j.atmosenv.2015.07.017.

Bikkina, S., Andersson, A., Kirillova, E.N., Holmstrand, H., Tiwari, S., Srivastava, A.K., Bisht, D.S., Gustafsson, Ö., 2019. Air quality in megacity Delhi affected by countryside biomass burning. Nat. Sustain 2, 200–205. https://doi.org/10.1038/s41893-019-0219-0.

Canagaratna, M.R., Jayne, J.T., Jimenez, J.L., Allan, J.D., Alfarra, M.R., Zhang, Q., Onasch, T.B., Drewnick, F., Coe, H., Middlebrook, A., Delia, A., Williams, L.R., Trimborn, A.M., Northway, M.J., DeCarlo, P.F., Kolb, C.E., Davidovits, P., Worsnop, D.R., 2007. Chemical and microphysical characterization of ambient aerosols with the aerodyne aerosol mass spectrometer. Mass Spectrom. Rev. 26, 185–222. https://doi.org/10.1002/Mas.20115.

Canagaratna, M.R., Jimenez, J.L., Kroll, J.H., Chen, Q., Kessler, S.H., Massoli, P., Hildebrandt Ruiz, L., Fortner, E., Williams, L.R., Wilson, K.R., Surratt, J.D., Donahue, N.M., Jayne, J.T., Worsnop, D.R., 2015. Elemental ratio measurements of organic compounds using aerosol mass spectrometry: characterization, improved calibration, and implications. Atmos. Chem. Phys. 15, 253–272. https://doi.org/10.5194/acp-15-253-2015.

Canonaco, F., Crippa, M., Slowik, J.G., Baltensperger, U., Prévôt, A.S.H., 2013. SoFi, an IGOR-based interface for the efficient use of the generalized multilinear engine (ME-2) for the source apportionment: ME-2 application to aerosol mass spectrometer data. Atmos. Meas. Tech 6, 3649–3661. https://doi.org/10.5194/amt-6-3649-2013.

Cheng, Y., He, K.-B., Zheng, M., Duan, F.-K., Du, Z.-Y., Ma, Y.-L., Tan, J.-H., Yang, F.-M., Liu, J.-M., Zhang, X.-L., Weber, R.J., Bergin, M.H., Russell, A.G., 2011. Mass absorption efficiency of elemental carbon and water-soluble organic carbon in Beijing, China. Atmos. Chem. Phys. 11, 11497–11510. https://doi.org/10.5194/acp-11-11497-2011.

Choudhary, V., Rajput, P., Singh, D.K., Singh, A.K., Gupta, T., 2018. Light absorption characteristics of brown carbon during foggy and non-foggy episodes over the Indo-Gangetic Plain. Atmos. Pollut. Res. 9, 494–501. https://doi.org/10.1016/j.apr.2017.11.012.

Crisp, T.A., Lerner, B.M., Williams, E.J., Quinn, P.K., Bates, T.S., Bertram, T.H., 2014. Observations of gas phase hydrochloric acid in the polluted marine boundary layer. J. Geophys. Res. Atmos. 119, 6897–6915. https://doi.org/10.1002/2013JD020992.

de Sá, S.S., Rizzo, L.V., Palm, B.B., Campuzano-Jost, P., Day, D.A., Yee, L.D., Wernis, R., Isaacman-VanWertz, G., Brito, J., Carbone, S., Liu, Y.J., Sedlacek, A., Springston, S., Goldstein, A.H., Barbosa, H.M.J., Alexander, M.L., Artaxo, P., Jimenez, J.L., Martin, S.T., 2019. Contributions of biomass-burning, urban, and biogenic emissions to the concentrations and light-absorbing properties of particulate matter in central Amazonia during the dry season. Atmos. Chem. Phys. 19, 7973–8001. https://doi.org/10.5194/acp-19-7973-2019.

Dasari, S., Andersson, A., Bikkina, S., Holmstrand, H., Budhavant, K., Satheesh, S., Asmi, E., Kesti, J., Backman, J., Salam, A., Bisht, D.S., Tiwari, S., Hameed, Z., Gustafsson, Ö., 2019. Photochemical degradation affects the light absorption of

water-soluble brown carbon in the South Asian outflow. Sci. Adv. https://doi.org/10.1126/sciadv.aau8066.
Drinovec, L., Močnik, G., Zotter, P., Prévôt, A., Ruckstuhl, C., Coz, E., Rupakheti, M., Sciare, J., Müller, T., Wiedensohler, A., 2015. The "dual-spot" Aethalometer: an improved measurement of aerosol black carbon with real-time loading compensation. Atmos. Meas. Tech 8, 1965–1979. https://doi.org/10.5194/amt-8-1965-2015.
Dumka, U.C., Tiwari, S., Kaskaoutis, D.G., Soni, V.K., Safai, P.D., Attri, S.D., 2019. Aerosol and pollutant characteristics in Delhi during a winter research campaign. Environ. Sci. Pollut. Res. Int. 26, 3771–3794. https://doi.org/10.1007/s11356-018-3885-y.
Ealo, M., Alastuey, A., Pérez, N., Ripoll, A., Querol, X., Pandolfi, M., 2018. Impact of aerosol particle sources on optical properties in urban, regional and remote areas in the northwestern Mediterranean. Atmos. Chem. Phys. 18, 1149–1169. https://doi.org/10.5194/acp-18-1149-2018.
Feng, Y., Ramanathan, V., Kotamarthi, V.R., 2013. Brown carbon: a significant atmospheric absorber of solar radiation? Atmos. Chem. Phys. 13, 8607–8621. https://doi.org/10.5194/acp-13-8607-2013.
Gani, S., Bhandari, S., Seraj, S., Wang, D.S., Patel, K., Soni, P., Arub, Z., Habib, G., Hildebrandt Ruiz, L., Apte, J.S., 2019. Submicron aerosol composition in the world's most polluted megacity: the Delhi Aerosol Supersite study. Atmos. Chem. Phys. 19, 6843–6859. https://doi.org/10.5194/acp-19-6843-2019.
Guttikunda, S.K., Calori, G., 2013. A GIS based emissions inventory at 1 km x 1 km spatial resolution for air pollution analysis in Delhi, India. Atmos. Environ 67, 101–111. https://doi.org/10.1016/j.atmosenv.2012.10.040.
Hallquist, M., Wenger, J.C., Baltensperger, U., Rudich, Y., Simpson, D., Claeys, M., Dommen, J., Donahue, N.M., George, C., Goldstein, A.H., Hamilton, J.F., Herrmann, H., Hoffmann, T., Iinuma, Y., Jang, M., Jenkin, M.E., Jimenez, J.L., Kiendler-Scharr, A., Maenhaut, W., McFiggans, G., Mentel, ThF., Monod, A., Prevot, A.S.H., Seinfeld, J.H., Surratt, J.D., Szmigielski, R., Wildt, J., 2009. The formation, properties and impact of secondary organic aerosol: current and emerging issues. Atmos. Chem. Phys. 9, 5155–5236. https://doi.org/10.5194/acp-9-5155-2009.
Hansen, A., Rosen, H., Novakov, T., 1984. The aethalometer—an instrument for the real-time measurement of optical absorption by aerosol particles. Sci. Total Environ. 36, 191–196. https://doi.org/10.1016/0048-9697(84)90265-1.
Herich, H., Hueglin, C., Buchmann, B., 2011. A 2.5 year's source apportionment study of black carbon from wood burning and fossil fuel combustion at urban and rural sites in Switzerland. Atmos. Meas. Tech 4, 1409–1420. https://doi.org/10.5194/amt-4-1409-2011.
Hu, W., Hu, M., Hu, W., Jimenez, J.L., Yuan, B., Chen, W., Wang, M., Wu, Y., Chen, C., Wang, Z., Peng, J., Zeng, L., Shao, M., 2016. Chemical composition, sources, and aging process of submicron aerosols in Beijing: contrast between summer and winter. J. Geophys. Res. Atmos. 121, 1955–1977. https://doi.org/10.1002/2015JD024020.
Ianniello, A., Spataro, F., Esposito, G., Allegrini, I., Hu, M., Zhu, T., 2011. Chemical characteristics of inorganic ammonium salts in $PM_{2.5}$ in the atmosphere of Beijing (China). Atmos. Chem. Phys. 11, 10803–10822. https://doi.org/10.5194/acp-11-10803-2011.
Kirchstetter, T.W., Novakov, T., Hobbs, P.V., 2004. Evidence that the spectral dependence of light absorption by aerosols is affected by organic carbon. J. Geophys. Res. Atmos. 109, 1–12. https://doi.org/10.1029/2004JD004999.
Kirillova, E.N., Andersson, A., Tiwari, S., Srivastava, A.K., Bisht, D.S., Gustafsson, Ö., 2014. Water-soluble organic carbon aerosols during a full New Delhi winter: isotope-based source apportionment and optical properties. J. Geophys. Res. Atmos. 119, 3476–3485. https://doi.org/10.1002/2013JD020041.
Laskin, A., Laskin, J., Nizkorodov, S.A., 2015. Chemistry of atmospheric brown carbon. Chem. Rev. 115, 4335–4382. https://doi.org/10.1021/cr5006167.
Lack, D.A., Langridge, J.M., 2013. On the attribution of black and brown carbon light absorption using the Ångström exponent. Atmos. Chem. Phys. 13, 10535–10543. https://doi.org/10.5194/acp-13-10535-2013.
Lin, G., Penner, J.E., Flanner, M.G., Sillman, S., Xu, L., Zhou, C., 2014. Radiative forcing of organic aerosol in the atmosphere and on snow: effects of SOA and brown carbon. J. Geophys. Res. Atmos. 119, 7453–7476. https://doi.org/10.1002/2013JD021186.
Lin, P., Huang, X.-F., He, L.-Y., Yu, J.Z., 2010. Abundance and size distribution of HULIS in ambient aerosols at a rural site in South China. J. Aerosol Sci. 41, 74–87. https://doi.org/10.1016/j.jaerosci.2009.09.001.
Lin, P., Liu, J., Shilling, J.E., Kathmann, S.M., Laskin, J., Laskin, A., 2015. Molecular characterization of brown carbon (BrC) chromophores in secondary organic aerosol generated from photo-oxidation of toluene. Phys. Chem. Chem. Phys. 17, 23312–23325. https://doi.org/10.1039/C5CP02563J.
Lu, Z., Streets, D.G., Winijkul, E., Yan, F., Chen, Y., Bond, T.C., et al., 2015. Light absorption properties and radiative effects of primary organic aerosol emissions. Environ. Sci. Technol. 49, 4868–4877. https://doi.org/10.1021/acs.est.5b00211.
Lukács, H., Gelencser, A., Hammer, S., Puxbaum, H., Pio, C.A., Legrand, M., Kasper-Giebl, A., Handler, M., Limbeck, A., Simpson, D., Preunkert, S., 2007. Seasonal trends and possible sources of brown carbon based on 2-year aerosol measurements at six sites in Europe. J. Geophys. Res. 112, 1–9. https://doi.org/10.1029/2006JD008151.
Massabò, D., Caponi, L., Bernardoni, V., Bove, M.C., Brotto, P., Calzolai, G., Cassola, F., Chiari, M., Fedi, M.E., Fermo, P., Giannoni, M., Lucarelli, F., Nava, S., Piazzalunga, A., Valli, G., Vecchi, R., Prati, P., 2015. Multi-wavelength optical determination of black and brown carbon in atmospheric aerosols. Atmos. Environ. 108, 1–12. https://doi.org/10.1016/j.atmosenv.2015.02.058.
Myhre, G., Samset, B.H., Schulz, M., Balkanski, Y., Bauer, S., Berntsen, T.K., Bian, H., Bellouin, N., Chin, M., Diehl, T., Easter, R.C., Feichter, J., Ghan, S.J., Hauglustaine, D., Iversen, T., Kinne, S., Kirkevåg, A., Lamarque, J.-F., Lin, G., Liu, X., Lund, M.T., Luo, G., Ma, X., van Noije, T., Penner, J.E., Rasch, P.J., Ruiz, A., Seland, Ø., Skeie, R.B., Stier, P., Takemura, T., Tsigaridis, K., Wang, P., Wang, Z., Xu, L., Yu, H., Yu, F., Yoon, J.-H., Zhang, K., Zhang, H., Zhou, C., 2013. Radiative forcing of the direct aerosol effect from AeroCom Phase II simulations. Atmos. Chem. Phys. 13, 1853–1877. https://doi.org/10.5194/acp-13-1853-2013.
Ng, N.L., Canagaratna, M.R., Jimenez, J.L., Chhabra, P.S., Seinfeld, J.H., Worsnop, D.R., 2011. Changes in organic aerosol composition with aging inferred from aerosol mass spectra. Atmos. Chem. Phys. 11, 6465–6474. https://doi.org/10.5194/acp-11-6465-2011.
Paatero, P., Tapper, U., 1994. Positive matrix factorization: a non-negative factor model with optimal utilization of error-estimates of data values. Environmetrics 5, 111–126. https://doi.org/10.1002/env.3170050203.
Paatero, P., 1999. The multilinear engine—a table-driven, least squares program for solving multilinear problems, including the n-way parallel factor Analysis model. J. Comput. Graph Stat. 8, 854–888. https://doi.org/10.1080/10618600.1999.10474853.
Pani, S.K., Wang, S.H., Lin, N.H., Chantara, S., Lee, C.T., Thepnuan, D., 2020. Black carbon over an urban atmosphere in northern peninsular Southeast Asia: characteristics, source apportionment, and associated health risks. Environ. Pollut. 259 (113871) https://doi.org/10.1016/j.envpol.2019.113871.
Puthussery, J., Singh, A., Rai, P., Bhattu, D., Kumar, V., Vats, P., Furger, M., Rastogi, N., Slowik, J., Ganguly, D., Prevot, A.S.H., Tripathi, S., Verma, V., 2020. Real-time measurements of PM2.5 oxidative potential using dithiothreitol (DTT) assay in Delhi, India. Environ. Sci. Technol. Lett. 7, 504–510. https://doi.org/10.1021/acs.estlett.0c00342.
Qin, Y.M., Tan, H.B., Li, Y.J., Li, Z.J., Schurman, M.I., Liu, L., Wu, C., Chan, C.K., 2018. Chemical characteristics of brown carbon in atmospheric particles at a suburban site near Guangzhou, China. Atmos. Chem. Phys. 18, 16409–16418. https://doi.org/10.5194/acp-18-16409-2018.
Rai, P., Furger, M., El Haddad, I., Kumar, V., Wang, L., Singh, A., Dixit, K., Bhattu, D., Petit, J.-E., Ganguly, D., Rastogi, N., Baltensperger, U., Tripathi, S., Slowik, J., Prevot, A.S.H., 2020. Real-time measurement and source apportionment of elements in Delhi's atmosphere. Sci. Total Environ. 742 https://doi.org/10.1016/j.scitotenv.2020.140332.
Ramana, M.V., Ramanathan, V., Feng, Y., Yoon, S.-C., Kim, S.-W., Carmichael, G.R., Schauer, J.J., 2010. Warming influenced by the ratio of black carbon to sulphate and the black-carbon source. Nat. Geosci. 3, 542–545. https://doi.org/10.1038/ngeo918.
Ran, L., Deng, Z.Z., Wang, P.C., Xia, X.A., 2016. Black carbon and wavelength-dependent aerosol absorption in the North China Plain based on two-year aethalometer measurements. Atmos. Environ. 142, 132–144. https://doi.org/10.1016/j.atmosenv.2016.07.014.
Rastogi, N., Singh, A., Satish, R.V., 2019. Characteristics of submicron particles coming from a big firecracker burning event: implications to atmospheric pollution. Atmos. Pollut. Res. 10, 629–634. https://doi.org/10.1016/j.apr.2018.11.002.
Rastogi, N., Agnihotri, R., Sawlani, R., Patel, A., Suresh Babu, S., Satish, R., 2020. Chemical and isotopic and characteristics of PM_{10} over the Bay of Bengal: effects of continental outflow on a marine environment. Sci. Total Environ. 726 (138438), DOI. https://doi.org/10.1016/j.scitotenv.2020.138438.
Russell, P.B., Bergstrom, R.W., Shinozuka, Y., Clarke, A.D., DeCarlo, P.F., Jimenez, J.L., Livingston, J.M., Redemann, J., Dubovik, O., Strawa, A., 2010. Absorption Angstrom Exponent in AERONET and related data as an indicator of aerosol composition. Atmos. Chem. Phys. 10, 1155–1169. https://doi.org/10.5194/acp-10-1155-2010.
Sandradewi, J., Prevot, A.S.H., Szidat, S., Perron, N., Alfarra, M.R., Lanz, V.A., Weingartner, E., Baltensperger, U., 2008. Using aerosol light absorption measurements for the quantitative determination of wood burning and traffic emission contributions to particulate matter. Environ. Sci. Technol. 42, 3316–3323. https://doi.org/10.1021/es702253m.
Satish, R., Shamjad, P., Thamban, N., Tripathi, S., Rastogi, N., 2017. Temporal characteristics of Brown carbon over the central Indo-Gangetic plain. Environ. Sci. Technol. 51, 6765–6772. https://doi.org/10.1021/acs.est.7b00734.
Satish, R., Rastogi, N., 2019. On the use of Brown carbon spectra as a tool to understand their broader composition and characteristics: a case study from crop-residue burning samples. ACS Omega 4, 1847–1853. https://doi.org/10.1021/acsomega.8b02637.
Satish, R., Rastogi, N., Singh, A., Singh, D., 2020. Change in characteristics of water-soluble and water-insoluble brown carbon aerosol during a large-scale biomass burning. Environ. Sci. Pollut. Res. 27, 33339–33350. https://doi.org/10.1007/s11356-020-09388-7.
Sembhi, H., Wooster, M., Zhang, T., Sharma, S., Singh, N., Agarwal, S., Boesch, H., Gupta, S., Misra, A., Tripathi, S.N., Mor, S., Khaiwal, R., 2020. Post-monsoon air quality degradation across Northern India: assessing the impact of policy-related 2 shifts in timing and amount of crop residue burnt. Environ. Res. Lett. 15 https://doi.org/10.1088/1748-9326/aba714.
Shamjad, P.M., Tripathi, S.N., Thambam, N.M., Vreeland, H., 2016. Refractive index and absorption attribution of highly absorbing Brown carbon aerosols from an urban Indian city-Kanpur. Sci. Rep. 6, 37735. https://doi.org/10.1038/srep37735.
Singh, A., Rajput, P., Sharma, D., Sarin, M.M., Singh, D., 2014. Black carbon and elemental carbon from post-harvest agricultural-waste burning emissions in the Indo-Gangetic Plain. Adv. Meteorol. 2014 https://doi.org/10.1155/2014/179301.
Singh, A., Rastogi, N., Patel, A., Satish, R.V., Singh, D., 2016. Size-segregated characteristics of carbonaceous aerosols over the northwestern Indo-Gangetic Plain: year round temporal behavior. Aerosol Air Qual. Res. 16, 1615–1624. https://doi.org/10.4209/aaqr.2016.01.0023.

Singh, A., Satish, R.V., Rastogi, N., 2019. Characteristics and sources of fine organic aerosol over a big semi-arid urban city of western India using HR-ToF-AMS. Atmos. Environ. 208, 103–112. https://doi.org/10.1016/j.atmosenv.2019.04.009.

Thamban, N., Joshi, B., Tripathi, S., Sueper, D., Canagaratna, M., Moosakutty, S., Satish, R., Rastogi, N., 2019. Evolution of aerosol size and composition in the Indo-Gangetic plain: size-resolved analysis of high-resolution aerosol mass spectra. ACS Earth Space Chem. 3, 823–832. https://doi.org/10.1021/acsearthspacechem.8b00207.

Tiwari, S., Srivastava, A.K., Bisht, D.S., Safai, P.D., Parmita, P., 2013. Assessment of carbonaceous aerosol over Delhi in the Indo-Gangetic Basin: characterization, sources and temporal variability. Nat. Hazards 65, 1745–1764. https://doi.org/10.1007/s11069-012-0449-1.

Tobler, A., Deepika, B., Canonaco, F., Lalchandani, V., Shukla, A., Thamban, N.M., Mishra, S., Srivastava, A.K., Bisht, D.S., Tiwari, S., Singh, S., Mocnik, G., Baltensperger, U., Tripathi, S.N., Slowik, J.G., Prévôt, A.S.H., 2020. Chemical characterization of $PM_{2.5}$ and source apportionment of organic aerosol in New Delhi, India. Sci. Total Environ 745. https://doi.org/10.1016/j.scitotenv.2020.140924.

Wang, L., Slowik, J.G., Tripathi, N., Bhattu, D., Rai, P., Kumar, V., Vats, P., Satish, R., Baltensperger, U., Ganguly, D., Rastogi, N., Sahu, L.K., Tripathi, S.N., Prévôt, A.S.H., 2020. Source characterization of volatile organic compounds measured by proton-transfer-reaction time-of-flight mass spectrometers in Delhi, India. Atmos. Chem. Phys. 20, 9753–9770. https://doi.org/10.5194/acp-20-9753-2020.

Wang, X., Heald, C.L., Ridley, D.A., Schwarz, J.P., Spackman, J.R., Perring, A.E., Coe, H., Liu, D., Clarke, A.D., 2014. Exploiting simultaneous observational constraints on mass and absorption to estimate the global direct radiative forcing of black carbon and brown carbon. Atmos. Chem. Phys. 14, 10989–11010. https://doi.org/10.5194/acp-14-10989-2014.

Xie, M., Chen, X., Hays, M.D., Lewandowski, M., Offenberg, J., Kleindienst, T.E., Holder, A.L., 2017. Light absorption of secondary organic aerosol: composition and contribution of nitroaromatic compounds. Environ. Sci. Technol. 51, 11607–11616. https://doi.org/10.1021/acs.est.7b03263.

Xie, M., Hays, M.D., Holder, A.L., 2018. Light-absorbing organic carbon from prescribed and laboratory biomass burning and gasoline vehicle emissions. Sci. Rep. 7 https://doi.org/10.1038/s41598-017-06981-8.

Yang, M., Howell, S.G., Zhuang, J., Huebert, B.J., 2009. Attribution of aerosol light absorption to black carbon, brown carbon, and dust in China – interpretations of atmospheric measurements during EAST-AIRE. Atmos. Chem. Phys. 9, 2035–2050. https://doi.org/10.5194/acp-9-2035-2009.

Yu, H., 2002. Environmental Carcinogenic polycyclic aromatic hydrocarbons: photochemistry and phototoxicity. J. Environ. Sci. Health C Environ. Carcinog. Ecotoxicol. Rev. 20, 149–183. https://doi.org/10.1081/GNC-120016203.

Zhang, Q., Jimenez, J.L., Worsnop, D.R., Canagaratna, M., 2007. A case study of urban particle acidity and its influence on secondary organic aerosol. Environ. Sci. Technol. 41, 3213–3219. https://doi.org/10.1021/es061812j.

Zhang, Q., Jimenez, J.L., Canagaratna, M.R., Ulbrich, I.M., Ng, N.L., Worsnop, D.R., Sun, Y., 2011. Understanding atmospheric organic aerosols via factor analysis of aerosol mass spectrometry: a review. Anal. Bioanal. Chem. 401, 3045–3067. https://doi.org/10.1007/s00216-011-5355-y.

Zhang, Y., Albinet, A., Petit, J.-E., Jacob, V., Chevrier, F., Gille, G., Pontet, S., Chrétien, E., Dominik-Sègue, M., Levigoureux, G., Močnik, G., Gros, V., Jaffrezo, J.-L., Favez, O., 2020. Substantial brown carbon emissions from wintertime residential wood burning over. France. Sci. Total Environ 743. https://doi.org/10.1016/j.scitotenv.2020.140752.

Zhu, C.-S., Cao, J.-J., Hu, T.-F., Shen, Z.-X., Tie, X.-X., Huang, H., Wang, Q.-Y., Huang, R.-J., Zhao, Z.-Z., Mocnik, G., Hansen, A.D.A., 2017. Spectral dependence of aerosol light absorption at an urban and a remote site over the Tibetan Plateau. Sci. Total Environ 590/591, 14–21. https://doi.org/10.1016/j.scitotenv.2017.03.057.